

# Superconducting and normal state properties of the layered boride OsB<sub>2</sub>

Yogesh Singh, A. Niazi, M. W. Vannette, R. Prozorov, and D. C. Johnston  
*Ames Laboratory and Department of Physics and Astronomy, Iowa State University, Ames, IA 50011*  
(Dated: December 2, 2024)

OsB<sub>2</sub> crystallizes in an orthorhombic structure (*Pmmn*) which contains alternate boron and osmium layers stacked along the *c*-axis. The boron layers consist of puckered hexagons as opposed to the flat graphite-like boron layers in MgB<sub>2</sub>. OsB<sub>2</sub> is reported to become superconducting below 2.1 K. We report results of the dynamic and static magnetic susceptibility, electrical resistivity, heat capacity and penetration depth measurements on arc-melted polycrystalline samples of OsB<sub>2</sub> to characterize its superconducting and normal state properties. These measurements confirmed that OsB<sub>2</sub> becomes a bulk superconductor below  $T_c = 2.1$  K. Our results indicate that OsB<sub>2</sub> is a moderate-coupling Type-II superconductor with an electron-phonon coupling constant  $\lambda_{ep} \approx 0.4\text{--}0.5$ , a small Ginzburg-Landau parameter  $\kappa \sim 2$  and an upper critical magnetic field  $H_{c2}(0.5\text{ K}) \sim 420$  Oe. The temperature dependence of the superfluid density  $n_s(T)$  is consistent with an *s*-wave superconductor with a slightly enhanced zero temperature gap  $\Delta(0) = 1.9 k_B T_c$  and a zero temperature London penetration depth  $\lambda(0) = 0.38(2) \mu\text{m}$ . The magnetic, transport and thermal properties in the normal state of isostructural and isoelectronic RuB<sub>2</sub>, which is reported to become superconducting below 1.6 K, are also reported. In the normal state OsB<sub>2</sub> and RuB<sub>2</sub> are Pauli paramagnetic metals with very similar properties: residual resistivity  $\rho_0 = 1.7(2)$  and  $1.1(1) \mu\Omega \text{ cm}$ ; Pauli susceptibility  $\chi_P = 3.4(5) \times 10^{-5}$  and  $5.22(7) \times 10^{-5} \text{ cm}^3/\text{mol}$ ; electronic specific heat coefficient  $\gamma = 1.90(1)$  and  $1.72(3) \text{ mJ/mol K}^2$ ; and low temperature  $T^3$  lattice specific heat coefficient  $\beta = 0.031(2)$  and  $0.015(1) \text{ mJ/mol K}^4$  for OsB<sub>2</sub> and RuB<sub>2</sub>, respectively. From our specific heat data, the density of states at the Fermi energy is  $N(\epsilon_F) = 1.1 \text{ states/(eV f.u.)}$  (f.u.  $\equiv$  formula unit) for OsB<sub>2</sub>.

## I. INTRODUCTION

Since the discovery of superconductivity in MgB<sub>2</sub> at a remarkably high temperature  $T_c \approx 39$  K,<sup>1</sup> there has been a renewed interest in the study of metal diborides. Many structurally-related TB<sub>2</sub> compounds ( $T = \text{Ti, Zr, Hf, V, Cr, Nb, Ta, Mo}$ ) have been investigated in the search for superconductivity,<sup>2,3,4</sup> some of which had already been studied in the past.<sup>5</sup>

Among all binary diborides with the AlB<sub>2</sub> structure, apart from MgB<sub>2</sub>, superconductivity has only been reported for ZrB<sub>2</sub> ( $T_c \approx 5.5$  K),<sup>3</sup> NbB<sub>2</sub> ( $T_c \approx 0.6$  K), Zr<sub>0.13</sub>Mo<sub>0.87</sub>B<sub>2</sub> ( $T_c \approx 5$  K)<sup>5</sup> and TaB<sub>2</sub> ( $T_c \approx 10$  K)<sup>2</sup> although there are controversies about superconductivity in ZrB<sub>2</sub>, NbB<sub>2</sub> and TaB<sub>2</sub>.<sup>3,4</sup> It has been argued using band structure calculations that in MgB<sub>2</sub>, the high  $T_c$  is due to the B 2p bands at the Fermi energy, and that any chemical, structural or other influence that changes this depresses  $T_c$ .<sup>6</sup> OsB<sub>2</sub> and RuB<sub>2</sub>, which form in an orthorhombic structure (*Pmmn*) containing deformed boron sheets instead of a planar boron array as in MgB<sub>2</sub>, have also been reported to become superconducting below 2.1 K and 1.6 K, respectively.<sup>7</sup> Recently the bulk modulus of OsB<sub>2</sub> at ambient and high pressure and its hardness have been studied.<sup>8</sup> Other physical properties of OsB<sub>2</sub> besides  $T_c$  have not yet been reported. Band structure calculations suggest that OsB<sub>2</sub> and RuB<sub>2</sub> are indeed metallic.<sup>9,10</sup>

For comparison, the structures of MgB<sub>2</sub> and OsB<sub>2</sub> are shown in Fig. 1. While MgB<sub>2</sub> has flat graphite-like sheets of boron separated by a layer of transition metal atoms in a hexagonal close packing arrangement [Fig. 1(a)],<sup>1</sup> the OsB<sub>2</sub> structure has sheets of a deformed two-dimensional

network of corrugated boron hexagons. The boron layers lie between two planar transition metal layers which are offset [Fig. 1(b)].<sup>9</sup>

Herein we report the dynamic and static magnetic susceptibility, specific heat, resistivity and penetration depth studies on OsB<sub>2</sub> to characterize its superconducting and normal state properties. We confirmed that OsB<sub>2</sub> is metallic and becomes superconducting below  $T_c = 2.1$  K. Our results indicate that OsB<sub>2</sub> is a moderate-coupling superconductor with an electron-phonon coupling constant  $\lambda_{ep} \approx 0.4\text{--}0.5$ , a small Ginzburg-Landau parameter  $\kappa \sim 2$  and an upper critical magnetic field  $H_{c2}(0.5\text{ K}) \sim 420$  Oe. We also report measurements on RuB<sub>2</sub> which shows similar normal state properties. The paper is organized as follows. Experimental details are given in Sec. II. The structural results are presented in Sec. III A. The normal state electrical resistivity, magnetic susceptibility and heat capacity data are given in Sec. III B and the superconducting properties are given in Sec. III C. The paper is concluded in Sec. IV.

## II. EXPERIMENTAL DETAILS

The binary phase diagram of the Os-B system has recently been investigated in detail and it has been shown that OsB<sub>2</sub> melts congruently at about 1870 °C.<sup>11</sup> Polycrystalline samples ( $\sim 1$  g) of OsB<sub>2</sub> used in this study were therefore prepared by arc-melting. The two OsB<sub>2</sub> samples for which the properties are reported here were prepared with starting materials of different purity. One sample (sample A) was prepared from Os powder (99.95%, Alfa Aesar) and B chunks (99.5%, Alfa Aesar). The magnetization of this sample showed the presence

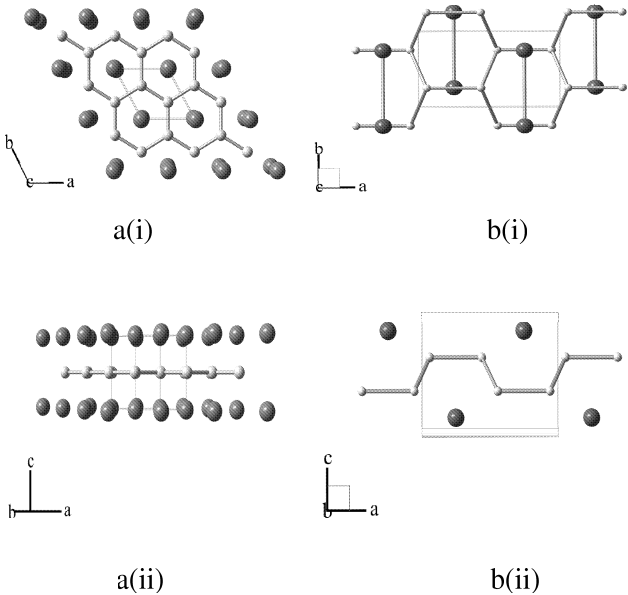


FIG. 1: The crystal structures of  $\text{MgB}_2$  (a) and  $\text{OsB}_2$  (b). The transition metal atoms are shown as large spheres while the boron atoms are shown as the small spheres. a(i) The  $\text{MgB}_2$  structure viewed along the  $c$ -axis and a(ii) perpendicular to the  $c$ -axis. The  $\text{MgB}_2$  structure has alternate boron and transition metals planes stacked along the  $c$ -axis. The boron atoms form graphite-like sheets in the  $ab$ -plane separated by a layer of transition metal atoms in a hexagonal close packing arrangement.<sup>1</sup> b(i) The  $\text{OsB}_2$  structure viewed along the  $c$ -axis and b(ii) viewed perpendicular to the  $c$ -axis. The  $\text{OsB}_2$  structure has a deformed two-dimensional network of corrugated boron hexagon sheets. Along the  $c$ -axis the boron layers lie between two planar transition metal layers which are offset along the  $ab$ -plane.<sup>9</sup>

of a large amount of paramagnetic impurities as apparent in the low temperature measurements. Therefore, another sample of  $\text{OsB}_2$  (sample B) was prepared using ultrahigh purity Os (99.995%, Sigma Aldrich) and  $^{11}\text{B}$  (99.999%, Eagle Pitcher). The magnetization for this sample showed that the concentration of paramagnetic impurities was considerably reduced compared to the first sample. The superconducting transition temperature and transition width are similar for these two samples. Most of the measurements pertaining to the superconducting state have been done on sample A while sample B has been used to obtain the intrinsic magnetic susceptibility of  $\text{OsB}_2$  and for  $^{11}\text{B}$  NMR measurements which will be reported elsewhere.

The samples were prepared as follows. The constituent elements were taken in stoichiometric proportion and arc-melted on a water-cooled copper hearth in high purity argon atmosphere. A Zr button was used as an oxygen getter. The sample was flipped over and remelted 10-15 times to ensure homogeneous mixing of the constituent elements. The mass of the ingot was checked after the initial two meltings and any weight loss due to the shattering of boron during melting was com-

sated by adding the appropriate amount of boron in subsequent melts. The arc-melted ingot so obtained had a shiny metallic luster with well formed crystal facets on the surface. A sample of the isostructural compound  $\text{RuB}_2$  was prepared similarly from high purity Ru powder (99.995%, MV labs) and  $^{11}\text{B}$  (99.999%, Eagle Pitcher). A portion of the as-cast samples was crushed for powder X-ray diffraction. Powder X-ray diffraction (XRD) patterns were obtained using a Rigaku Geigerflex diffractometer with  $\text{Cu K}\alpha$  radiation, in the  $2\theta$  range from 10 to  $90^\circ$  with a  $0.02^\circ$  step size. Intensity data were accumulated for 5 s per step.

Samples of starting composition  $\text{OsB}_{1.9}$  and  $\text{OsB}_{2.1}$  were also prepared with the above starting materials from Alfa Aesar. Powder X-ray diffraction measurements on crushed pieces of these samples showed that  $\text{OsB}_{1.9}$  is a two-phase sample containing the phases  $\text{Os}_2\text{B}_3$  and  $\text{OsB}_2$  while the  $\text{OsB}_{2.1}$  sample contained the phase  $\text{OsB}_2$  and elemental osmium. The purpose of making these samples was to explore both the boron-deficient and boron-rich sides, respectively, of the homogeneity range of  $\text{OsB}_2$ , if any, and its influence on the superconducting properties.

The temperature dependence of the dc magnetic susceptibility and isothermal magnetization was measured using a commercial Superconducting Quantum Interference Device (SQUID) magnetometer (MPMS5, Quantum Design). The resistivity and heat capacity were measured using a commercial Physical Property Measurement System (PPMS, Quantum Design). The magnetic susceptibility measurements were done on samples of arbitrary shape. The magnetization  $M$  versus field  $H$  measurements in Fig. 9 below were performed on a parallelepiped sample with dimensions: length = 3.25 mm, width = 1.57 mm and thickness = 0.35 mm with the magnetic field applied parallel to the length of the sample to minimize demagnetization effects. The  $M(H)$  loops in Fig. 10 below were measured with the field applied either parallel and perpendicular to the length of the sample. The resistance was measured using a four-probe technique with a current of 5 mA along the long axis of the rectangular bar, corresponding to a current density of  $0.91 \text{ A/cm}^2$ .

The dynamic susceptibility was measured between 0.5 K and 2.5 K using a 10 MHz tunnel-diode driven oscillator (TDO) circuit with a volume susceptibility sensitivity  $\Delta\chi \approx 10^{-8}$ .<sup>12</sup> For superconductors, this is equivalent to a change in the London penetration depth of about 0.5 Å for millimeter-sized samples.<sup>12,13,14</sup> A TDO is an  $LC$  tank circuit with a coil of inductance  $L$  and a capacitor  $C$ . The circuit is self-resonating at a frequency  $2\pi f = 1/\sqrt{LC}$ . When a sample with susceptibility  $\chi$  is inserted into the coil, the total inductance decreases for a diamagnetic sample or increases for a paramagnetic sample. The resonant frequency changes accordingly by an amount which is proportional to  $\chi$ .<sup>12</sup> Specifically, the device measures the temperature dependence of the resonant frequency shift  $\Delta f(T)$  induced by changes in the sample's magnetic response. The magnetic susceptibility

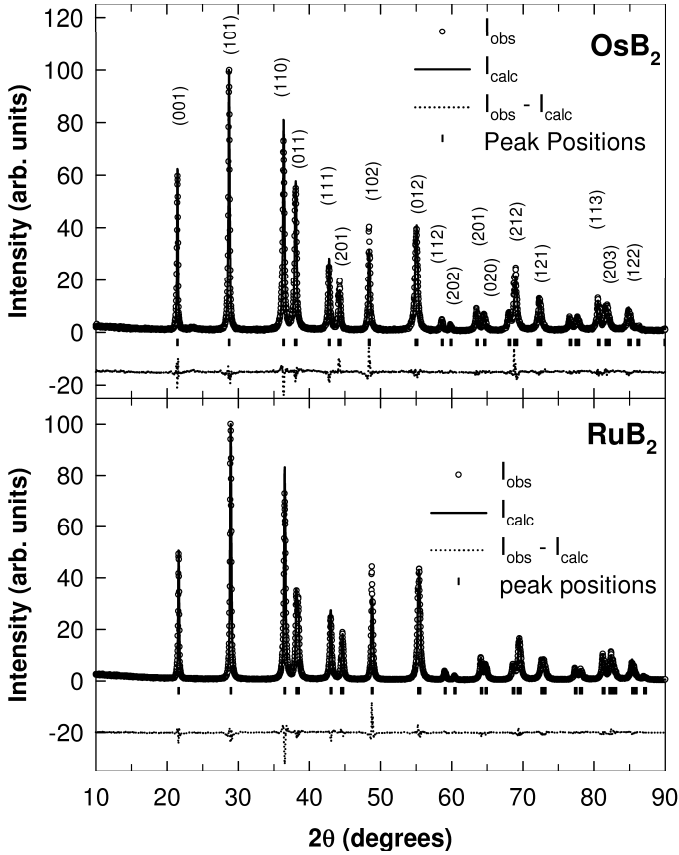


FIG. 2: Rietveld refinements of the OsB<sub>2</sub> and RuB<sub>2</sub> X-ray diffraction data. The open symbols represent the observed X-ray pattern, the solid lines represent the fitted pattern, the dotted lines represent the difference between the observed and calculated intensities and the vertical bars represent the peak positions.

$\chi$  is then given by<sup>14</sup>

$$\Delta f(T) = -4\pi\chi(T)G \approx -G \left[ 1 - \frac{\lambda(T)}{R} \tanh \left( \frac{R}{\lambda(T)} \right) \right] \quad (1)$$

where  $G$  is a sample-shape and coil-dependent calibration parameter,  $R$  is the effective sample dimension and  $\lambda(T)$  is the London penetration depth. The  $G$  has been determined by matching the temperature dependence of the skin depth obtained from the resonator response in the normal state of OsB<sub>2</sub> to the measured resistivity data.

### III. RESULTS

#### A. Structures of OsB<sub>2</sub> and RuB<sub>2</sub>

All the lines in the X-ray patterns for OsB<sub>2</sub> and RuB<sub>2</sub> could be indexed to the known orthorhombic *Pmmn* (No. 59) structure and Rietveld refinements,<sup>15</sup> shown in Fig. 2, of the X-ray patterns gave the lattice parameters

$a = 4.6851(6)$  Å,  $b = 2.8734(4)$  Å and  $c = 4.0771(5)$  Å for OsB<sub>2</sub> and  $a = 4.6457(5)$  Å,  $b = 2.8657(3)$  Å and  $c = 4.0462(4)$  Å for RuB<sub>2</sub>. These values are in excellent agreement with previously reported values.<sup>16</sup> The best fits were obtained when the anisotropic thermal parameters for the transition metal atom were allowed to vary. For boron the overall isotropic thermal parameter was fixed to zero because unphysically large values were obtained when it was allowed to vary and fixing it to zero did not change the quality of the fit. This is probably because the atomic number of boron is much less than that of either Os or Ru. A neutron diffraction study is needed to obtain reliable estimates of the thermal parameters for boron. Some parameters obtained from the Rietveld refinement are given in Table I. Although the lattice parameters and fractional atomic positions that we obtain from the Rietveld refinements for both OsB<sub>2</sub> and RuB<sub>2</sub> agree reasonably well with the earlier structural report,<sup>16</sup> the fits consistently underestimate the intensities of the (102) peaks at  $2\theta = 48.35^\circ$  (see Fig. 2).

#### B. Normal State Properties of OsB<sub>2</sub> and RuB<sub>2</sub>

##### 1. Electrical Resistivity

The electrical resistivity ( $\rho$ ) versus temperature of OsB<sub>2</sub> (sample A) and RuB<sub>2</sub> from 1.75 K to 300 K is shown in Fig. 3. The room temperature resistivity values are 36(3)  $\mu\Omega$  cm for OsB<sub>2</sub> and 53(5)  $\mu\Omega$  cm for RuB<sub>2</sub>. The error in the resistivity comes primarily from the error in the determination of the geometrical factors. Both compounds show metallic behavior with an approximately linear decrease in resistivity on cooling from room temperature. At low temperatures  $\rho$  becomes only weakly temperature dependent and reaches a residual resistivity  $\rho_0$  of 1.7(2)  $\mu\Omega$  cm just above 2.2 K for OsB<sub>2</sub> and 1.1(1)  $\mu\Omega$  cm at 1.8 K for RuB<sub>2</sub> as seen in the inset of Fig. 3. The large residual resistivity ratios RRR =  $\rho(300 \text{ K})/\rho_0$  = 22 for OsB<sub>2</sub> and RRR = 51 for RuB<sub>2</sub> indicate well-crystallized homogeneous samples. For OsB<sub>2</sub> the resistivity drops abruptly below 2.2 K and reaches zero by 2.12 K, as highlighted in the inset of Fig. 3. The superconducting properties will be discussed in detail in Sec. III C.

##### 2. Magnetic Susceptibility

Both OsB<sub>2</sub> and RuB<sub>2</sub> are so weakly magnetic that even trace amounts (few ppm) of magnetic impurities are apparent in the low temperature susceptibility and magnetization  $M(H)$  measurements. The  $M(H)$  data for OsB<sub>2</sub> at 1.8 K, 3.5 K and 5 K are shown in Fig. 4(a). The data were fitted by the expression

TABLE I: Structure parameters for  $\text{OsB}_2$  and  $\text{RuB}_2$  refined from powder XRD data.  $B_{11}$ ,  $B_{22}$  and  $B_{33}$  are the anisotropic thermal parameters defined within the thermal parameter of the intensity as  $e^{-(B_{11}h^2+B_{22}k^2+B_{33}l^2)}$ .

Sample	atom	$x$	$y$	$z$	$B_{11}$ ( $\text{\AA}^2$ )	$B_{22}$ ( $\text{\AA}^2$ )	$B_{33}$ ( $\text{\AA}^2$ )	$R_{\text{wp}}/R_{\text{p}}$
$\text{OsB}_2$	Os	0.25	0.25	0.1515(3)	0.0209(9)	0.045(2)	0.001(1)	1.39
	B	0.093(3)	0.25	0.669(4)				
$\text{RuB}_2$	Ru	0.25	0.25	0.1490(2)	0.0166(7)	0.051(2)	0.0007(9)	1.36
	B	0.063(1)	0.25	0.638(2)				

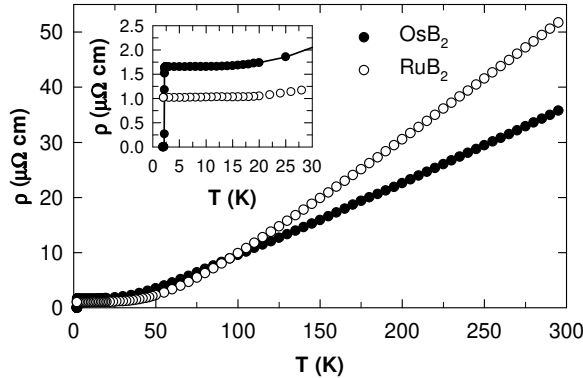


FIG. 3: Electrical resistivity  $\rho$  for  $\text{OsB}_2$  and  $\text{RuB}_2$  versus temperature  $T$ . The inset shows the low temperature data on an expanded scale to highlight the low residual resistivity.

$$M(H) = \chi_0 H + f N_A g S \mu_B B_S(x) \equiv \chi_0 H + M_{\text{Para}}(H) , \quad (2)$$

where  $\chi_0$  is the intrinsic susceptibility of  $\text{OsB}_2$ ,  $f$  is the molar fraction of paramagnetic impurities,  $N_A$  is Avogadro's number,  $g$  is the  $g$ -factor of the impurity spins,  $S$  is the spin of the paramagnetic impurities and  $B_S(x)$  is the Brillouin function where the argument  $x$  of the Brillouin function is  $x = g\mu_B S H / (T - \theta)$  where  $\theta$  is the Weiss temperature. The  $g$  value was fixed to two. The fitting parameters were  $\chi_0$ ,  $f$ ,  $S$  and  $\theta$  and we obtained  $\chi_0 = -6.09(1) \times 10^{-5} \text{ cm}^3/\text{mol}$ ,  $f = 1.57(4) \times 10^{-5}$ ,  $S = 1.54(6)$  and  $\theta = -1.8(2) \text{ K}$ . The fit is shown as the solid curves in Fig. 4(a). By subtracting from the observed  $M(H)$  data the  $\chi_0 H$  obtained from the fitting, one can obtain the contribution from paramagnetic impurities  $M_{\text{Para}}$  as shown in Fig. 4(b). The solid curves in Fig. 4(b) are the paramagnetic impurity part of the fit [the second term in Eq. (2)].

The normal state susceptibility  $\chi \equiv M/H$  for  $\text{OsB}_2$  and  $\text{RuB}_2$  has been measured versus temperature  $T$  between 1.8 K and 300 K in a field of 2 T and 5 T, respectively, as shown in Fig. 5. The  $\chi(T)$  for both samples is weakly temperature dependent between 50 K and 300 K. For  $\text{OsB}_2$ , below 50 K  $\chi(T)$  drops slightly on cooling, amounting to about 4% of the room temperature value. The upturn at low temperatures seen for both samples is

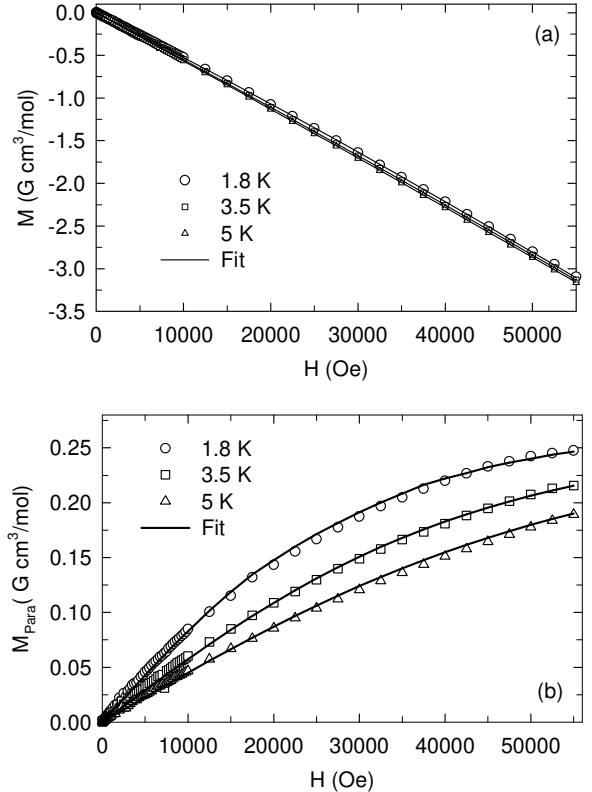


FIG. 4: (a) The magnetization  $M$  versus applied magnetic field  $H$  for  $\text{OsB}_2$  (sample B). The solid curves are fits by Eq. (2). (b) The paramagnetic impurity contribution  $M_{\text{Para}}$  to the total  $M(H)$ . The solid curves are the paramagnetic impurity part of Eq. (2).

most likely due to the presence of small amounts (a few ppm) of paramagnetic impurities as determined above for  $\text{OsB}_2$  ( $f = 16$  molar ppm). Figure 5(a) also shows the susceptibility after subtracting the paramagnetic impurity contribution  $\chi_{\text{Para}} = M_{\text{Para}}/H$  from the observed  $\chi$ .

The intrinsic susceptibility after subtracting  $\chi_{\text{Para}}$ ,  $\chi(T)$ , can be written as

$$\chi = \chi_{\text{core}} + \chi_L + \chi_{\text{VV}} + \chi_P , \quad (3)$$

where  $\chi_{\text{core}}$  is the diamagnetic orbital contribution from

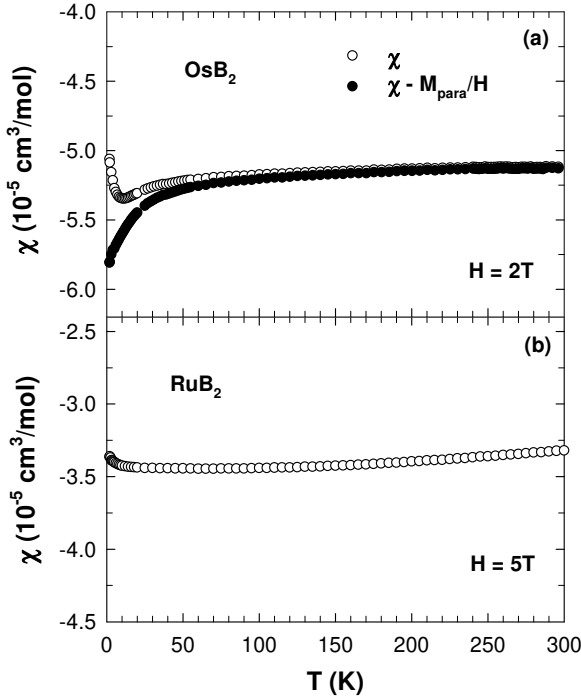


FIG. 5: Magnetic susceptibility  $\chi$  (open circles) versus temperature  $T$  for OsB<sub>2</sub> (a) and RuB<sub>2</sub> (b). In (a), the filled circles are the values obtained after subtracting the paramagnetic impurity contribution (see text).

the electrons (ionic or atomic),  $\chi_L$  is the Landau orbital diamagnetism of the conduction electrons,  $\chi_{VV}$  is the Van Vleck paramagnetic orbital contribution and  $\chi_P$  is the Pauli paramagnetic spin susceptibility of the conduction electrons. For OsB<sub>2</sub> and RuB<sub>2</sub>, the net diamagnetic susceptibility indicates quasi-free electrons with  $\chi_L = -(\frac{m}{m^*})^2 \frac{\chi_P}{3}$  and  $\chi_{VV} \approx 0$ ,<sup>17</sup> where  $m$  is the free electron mass and  $m^*$  is the effective mass of the current carriers. Assuming  $m^* = m$ , the Pauli susceptibility can be written as

$$\chi_P = \frac{3}{2}(\chi - \chi_{\text{core}}), \quad (4)$$

which can be extracted from the experimentally measured susceptibility, after correction for the paramagnetic impurity contribution, if the contribution from the core  $\chi_{\text{core}}$  is known. In covalent metals it is difficult to correctly estimate  $\chi_{\text{core}}$  because its value depends on the local electron density on the atoms. In an ionic model,  $\chi_{\text{core}} = -18 \times 10^{-6} \text{ cm}^3/\text{mol}$  for Os<sup>6+</sup> and  $-44 \times 10^{-6} \text{ cm}^3/\text{mol}$  for Os<sup>2+</sup>.<sup>18</sup> However if we use the ionic core diamagnetism values for Os and B, one obtains from Eq. (4) an unphysical negative  $\chi_P$ . For OsB<sub>2</sub> it is reasonable to use atomic (covalent) estimates of  $\chi_{\text{core}}$  instead of ionic values because the bonding in OsB<sub>2</sub> has a strong covalent character.<sup>19</sup> Therefore using the atomic diamagnetism values  $\chi_{\text{core}}$  for Os ( $-53.82 \times 10^{-6} \text{ cm}^3/\text{mol}$ ), Ru ( $-42.89 \times 10^{-6} \text{ cm}^3/\text{mol}$ ) and B ( $-12.55 \times 10^{-6} \text{ cm}^3/\text{mol}$ ),<sup>20</sup> we obtain  $\chi_{\text{core}} = -78 \times$

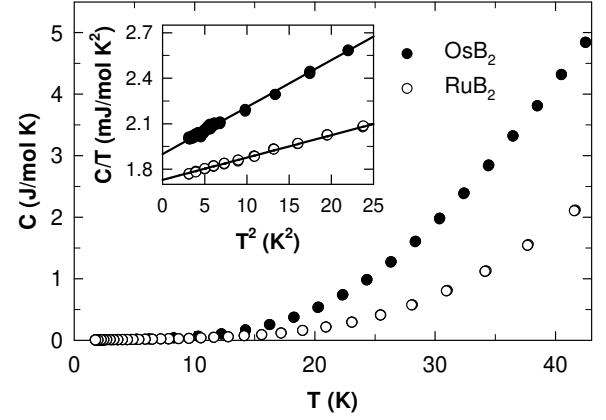


FIG. 6: The heat capacity  $C$  versus temperature  $T$  of OsB<sub>2</sub> and RuB<sub>2</sub> between 1.8 K and 45 K. The inset shows the data plotted as  $C/T$  versus  $T^2$  between 1.8 K and 5 K. The solid straight lines are fits by the expression  $C/T = \gamma + \beta T^2$ .

$10^{-6} \text{ cm}^3/\text{mol}$  for OsB<sub>2</sub> and  $\chi_{\text{core}} = -68 \times 10^{-6} \text{ cm}^3/\text{mol}$  for RuB<sub>2</sub>. Subtracting these values and the paramagnetic impurity contribution from the total measured susceptibility and accounting for the Landau diamagnetism, one can get the Pauli paramagnetic susceptibility using Eq. (4), thus yielding an average  $\chi_P = 3.4(5) \times 10^{-5} \text{ cm}^3/\text{mol}$  for OsB<sub>2</sub>.

From  $\chi_P$  one can estimate the density of states at the Fermi level  $N(\epsilon_F)$  for both spin directions using the relation

$$\chi_P = \mu_B^2 N(\epsilon_F), \quad (5)$$

where  $\mu_B$  is the Bohr magneton. Taking the above average value of  $\chi_P$  for OsB<sub>2</sub>, we get  $N(\epsilon_F) = 2.2(3)$  states/(eV f.u.), where “f.u.” means “formula unit”. This value is larger than the value from band structure calculations [ $N(\epsilon_F) \approx 0.55$  states/(eV f.u.)].<sup>9</sup> Similarly, from the average value of  $\chi_P = 5.22(7) \times 10^{-5} \text{ cm}^3/\text{mol}$  for RuB<sub>2</sub> one estimates using Eq. (5),  $N(\epsilon_F) = 3.0(2)$  states/(eV f.u.). This value is also larger than the value obtained from the band structure calculations [ $N(\epsilon_F) \approx 0.53$  states/(eV f.u.)].<sup>9</sup> The discrepancy between experiment and theory for OsB<sub>2</sub> is discussed later in terms of the Stoner enhancement factor of the susceptibility.

### 3. Heat Capacity

Figure 6 shows the results of the normal state heat capacity versus temperature  $C(T)$  measurements on OsB<sub>2</sub> (sample A) and RuB<sub>2</sub>, plotted as  $C$  versus  $T$ . The OsB<sub>2</sub> data were recorded in an applied magnetic field of 1 kOe to suppress the superconducting transition to below 1.75 K, which is the low-temperature limit of our measurements. The inset in Fig. 6 shows the low temperature data for both samples plotted as  $C/T$  versus  $T^2$ . The low temperature data (1.75 K to 5 K) for both

samples could be fitted by the expression  $C = \gamma T + \beta T^3$  where the first term is the contribution from the conduction electrons and the second term is the contribution from the lattice. The fits are shown as the solid straight lines in the inset of Fig. 6. The values

$$\gamma = 1.90(1) \text{ mJ/mol K}^2 \text{ and } \beta = 0.031(2) \text{ mJ/mol K}^4 \quad (6)$$

are obtained for  $\text{OsB}_2$  and the values

$$\gamma = 1.72(3) \text{ mJ/mol K}^2 \text{ and } \beta = 0.015(1) \text{ mJ/mol K}^4 \quad (7)$$

are obtained for  $\text{RuB}_2$ . From the values of  $\beta$ , one can obtain the Debye temperature  $\Theta_D$  using the expression<sup>21</sup>

$$\Theta_D = \left( \frac{12\pi^4 R n}{5\beta} \right)^{1/3}, \quad (8)$$

where  $R$  is the molar gas constant and  $n$  is the number of atoms per formula unit ( $n = 3$  for  $\text{OsB}_2$  and  $\text{RuB}_2$ ). We obtain  $\Theta_D = 550(11)$  K for  $\text{OsB}_2$  and  $\Theta_D = 701(14)$  K for  $\text{RuB}_2$ . A simple harmonic oscillator model predicts  $\Theta_D \propto (\frac{1}{M})^{1/2}$  (Ref. 21) where  $M$  is the molar mass of the compound. The ratio  $\frac{\Theta_D(\text{OsB}_2)}{\Theta_D(\text{RuB}_2)} = 0.79(3)$  is indeed close to the square root of the ratio of the molar masses  $\sqrt{\frac{M(\text{RuB}_2)}{M(\text{OsB}_2)}} = 0.76$ .

Another quantity which characterizes a metal is the ratio of the density of states as probed by magnetic measurements to the density of states probed by heat capacity measurements, which is the Wilson ratio

$$R_W = \frac{\pi^2 k_B^2}{3\mu_B^2} \left( \frac{\chi_P}{\gamma} \right). \quad (9)$$

For a free-electron Fermi gas  $R_W = 1$ . Using  $\chi_P = 3.4(5) \times 10^{-5} \text{ cm}^3/\text{mol}$  and  $\gamma = 1.90(1) \text{ mJ/mol K}^2$  for  $\text{OsB}_2$  we get  $R_W = 1.3(2)$  which is of the order of unity expected for a quasi-free electron gas. For  $\text{RuB}_2$ ,  $\chi_P = 5.22(7) \times 10^{-5} \text{ cm}^3/\text{mol}$  and  $\gamma = 1.72(3) \text{ mJ/mol K}^2$  which gives  $R_W = 2.21(7)$ .

### C. Superconducting Properties of $\text{OsB}_2$

#### 1. Electrical Resistivity and Heat Capacity Measurements

The results of the resistivity  $\rho(T)$  and heat capacity  $C(T)$  measurements at low temperatures are shown in Fig. 7 to highlight the superconducting transition. Figure 7(a) shows the low temperature resistivity  $\rho(T)$  data measured with various applied magnetic fields. In the zero field data there is an abrupt drop below 2.2 K and  $\rho$  reaches zero at  $T_c = 2.14$  K. The transition is quite sharp with a transition width (10% to 90%) of 60 mK. The superconducting transition is suppressed to lower temperatures in a magnetic field as can be seen in Fig. 7(a). We will return to these data when we estimate the critical field.

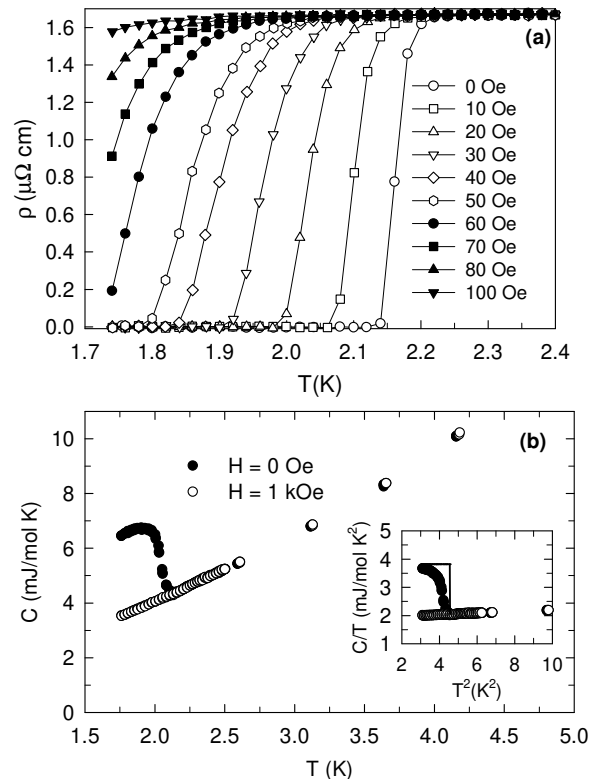


FIG. 7: (a) The resistivity  $\rho(T)$  of  $\text{OsB}_2$  between 1.7 K and 2.4 K measured with various applied magnetic fields. (b) Temperature dependence of the heat capacity  $C(T)$  of  $\text{OsB}_2$  in zero and 1 kOe applied magnetic field. The inset shows the data plotted as  $C/T$  versus  $T^2$ . The solid line in a construction to estimate the magnitude of the superconducting anomaly (see text for details).

Figure 7(b) shows the  $C(T)$  data measured in zero and 1 kOe applied field. The sharp anomaly at 2.1 K seen in the heat capacity data taken in zero applied field confirms the bulk nature of the superconductivity in  $\text{OsB}_2$ . The transition is completely suppressed to below 1.7 K in 1 kOe as seen in Fig. 7(b). The inset in Fig. 7(b) shows the data plotted as  $C/T$  versus  $T^2$ . The jump in the specific heat  $\Delta C$  at the superconducting transition  $T_c$  is usually normalized as  $\Delta C/\gamma T_c$  where  $\gamma$  is Sommerfeld's coefficient. Since the anomaly at the superconducting transition is somewhat broad and the temperature range below  $T_c$  is insufficient, we estimate  $\Delta C$  by constructing a transition at  $T_c$  with a  $\Delta C$  equal to the maximum of the superconducting anomaly in  $C/T$ . This is shown as the solid vertical line in the inset of Fig. 7(b). Using this value of  $\Delta C/T_c = 1.78 \text{ mJ/mol K}^2$  and  $\gamma = 1.90(1) \text{ mJ/mol K}^2$  obtained in the previous section we get  $\Delta C/\gamma T_c = 0.94$ . This is reduced from the value 1.43 expected from BCS theory. The origin of this suppression is not currently known. A reduced specific heat anomaly at the superconducting transition ( $\Delta C/\gamma T_c \sim 1$ ) is also observed in the two-gap superconductor  $\text{MgB}_2$ .<sup>22</sup> To evaluate this question in  $\text{OsB}_2$  re-

quires  $C(T)$  data to lower temperatures than in Fig. 7(b). However, we reiterate that the large specific heat jump at  $T_c$  demonstrates the bulk nature of the superconductivity in OsB<sub>2</sub>.

We now estimate the electron-phonon coupling constant  $\lambda_{\text{ep}}$ , using McMillan's formula<sup>23</sup> which relates the superconducting transition temperature  $T_c$  to  $\lambda_{\text{ep}}$ , the Debye temperature  $\Theta_D$ , and the Coulomb repulsion constant  $\mu^*$ ,

$$T_c = \frac{\Theta_D}{1.45} \exp \left[ -\frac{1.04(1 + \lambda_{\text{ep}})}{\lambda_{\text{ep}} - \mu^*(1 + 0.62\lambda_{\text{ep}})} \right], \quad (10)$$

which can be inverted to give  $\lambda_{\text{ep}}$  in terms of  $T_c$ ,  $\Theta_D$  and  $\mu^*$  as

$$\lambda_{\text{ep}} = \frac{1.04 + \mu^* \ln(\frac{\Theta_D}{1.45T_c})}{(1 - 0.62\mu^*) \ln(\frac{\Theta_D}{1.45T_c}) - 1.04}. \quad (11)$$

From the above heat capacity measurements we had obtained  $\Theta_D = 550(11)$  K and using  $T_c = 2.1$  K we get  $\lambda_{\text{ep}} = 0.41$  and  $0.5$  for  $\mu^* = 0.10$  and  $0.15$ , respectively. These values of  $\lambda_{\text{ep}}$  suggest that OsB<sub>2</sub> is a moderate-coupling superconductor ( $\lambda_{\text{ep}}$  for MgB<sub>2</sub> is  $\approx 1$ ).<sup>24</sup>

Having estimated  $\lambda_{\text{ep}}$ , the density of states at the Fermi energy for both spin directions  $N(\epsilon_F)$  can be estimated from the values of  $\gamma$  and  $\lambda_{\text{ep}}$  using the relation<sup>21</sup>

$$\gamma = \frac{\pi^2}{6} k_B^2 N(\epsilon_F)(1 + \lambda_{\text{ep}}) \equiv \gamma_0(1 + \lambda_{\text{ep}}). \quad (12)$$

We find  $N(\epsilon_F) = 1.14$  and  $1.06$  states/(eV f.u.) for  $\lambda_{\text{ep}} = 0.41$  and  $0.5$ , respectively. These values are larger than the value estimated by band structure calculations  $N(\epsilon_F) \approx 0.55$  (states/eV f.u.).<sup>9</sup> The bare Sommerfeld coefficient with  $\lambda_{\text{ep}} = 0.5$  is  $\gamma_0 = 1.4$  mJ/mol K<sup>2</sup>.

One can now go back and re-evaluate the Wilson ratio  $R_W$ . For a free electron Fermi gas  $R_W = 1$ . In Sec. III B, using the experimentally observed values of  $\chi_P$  and  $\gamma$  we had estimated  $R_W = 1.3$  for OsB<sub>2</sub>. However, the electron-phonon interaction leads to an enhancement in  $\gamma$  from its value  $\gamma_0$  in the absence of interactions given by  $\gamma = \gamma_0(1 + \lambda_{\text{ep}})$ . Similarly electron-electron interactions lead to an enhancement in the Pauli susceptibility  $\chi_P$  from its value  $\chi_P^0$  in the absence of interactions, given by  $\chi_P = \frac{\chi_P^0}{1-\alpha}$ , where  $\alpha$  is the Stoner enhancement factor. The re-evaluated Wilson ratio is then given by

$$R_W = \frac{\pi^2 k_B^2}{3\mu_B^2} \left( \frac{\chi_P^0}{\gamma_0} \right) = 1 = \frac{\pi^2 k_B^2}{3\mu_B^2} \left( \frac{\chi_P}{\gamma} \right) (1-\alpha)(1+\lambda_{\text{ep}}). \quad (13)$$

Using  $\lambda_{\text{ep}} = 0.5$  obtained in Sec. III B, one gets an estimate of the Stoner enhancement factor  $\alpha = 0.49$ .

## 2. dc Magnetization and ac Susceptibility

The temperature dependence of the zero-field-cooled (ZFC) and field-cooled (FC) dimensionless dc volume

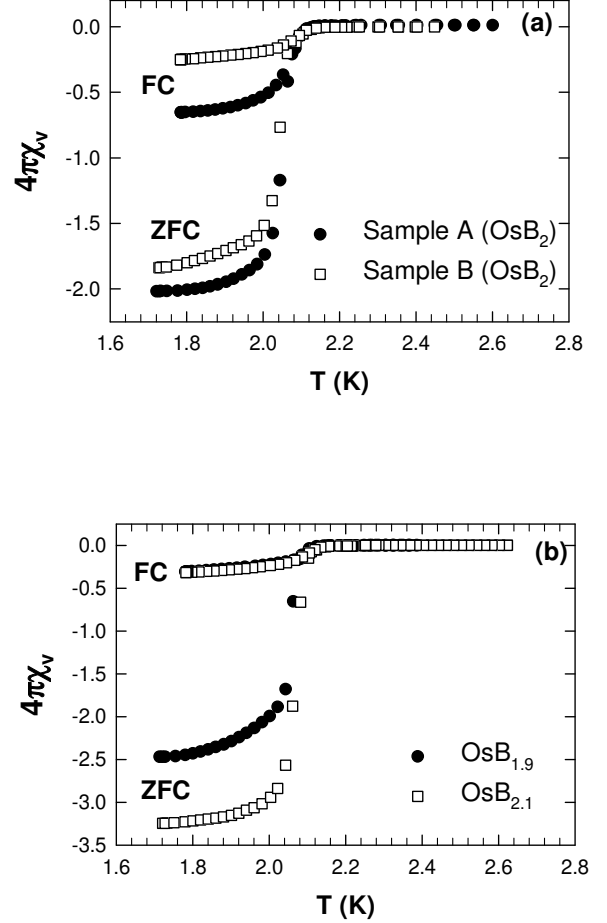


FIG. 8: Temperature  $T$  dependence of the zero-field-cooled (ZFC) and field-cooled (FC) volume susceptibility  $\chi_v$  in terms of the superconducting volume fraction ( $4\pi\chi_v$ ) of OsB<sub>2</sub> (Sample A and Sample B) (a) and OsB<sub>1.9</sub> and OsB<sub>2.1</sub> (b) in a field of 5 Oe from 1.7 to 2.6 K.

magnetic susceptibility  $\chi_v$  of OsB<sub>2</sub> samples A and B in a field of 5 Oe from 1.7 to 2.8 K is plotted in Fig. 8(a), where  $\chi_v = M_v/H$  and  $M_v$  is the volume magnetization. Complete diamagnetism corresponds to  $\chi_v = -1/4\pi$ , so the data have been normalized by  $1/4\pi$ . The data have not been corrected for the demagnetization factor  $N$  which gives  $\chi_v = \frac{-1/4\pi}{1-N}$  for the measured value. A sharp diamagnetic drop in the susceptibility below  $T_c = 2.14$  K for both samples signals the transition into the superconducting state. The width of the transition (10% to 90% of the transition) is 50 mK for sample A and 70 mK for sample B.

In Fig. 8(b) the temperature dependence of the susceptibility of the samples with composition OsB<sub>1.9</sub> and OsB<sub>2.1</sub> is shown. It can be seen that the onset temperature for the superconducting transition for both the samples is 2.1 K. This indicates that the homogeneity range of OsB<sub>2</sub>, if any, does not have any significant effect on the  $T_c$  of OsB<sub>2</sub>. All other measurements were therefore done on the single phase samples A and B of OsB<sub>2</sub>.

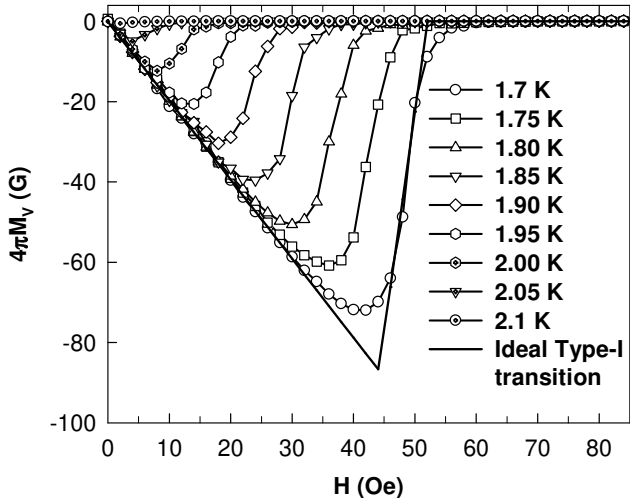


FIG. 9: Volume Magnetization ( $M_v$ ) normalized by  $1/4\pi$ , versus applied magnetic field ( $H$ ) at various temperatures.

To further characterize the superconducting state we have performed measurements of the dc magnetization versus field  $M(H)$  at various temperatures. The volume magnetization  $M_v(H)$  normalized by  $1/4\pi$  is shown in Fig. 9. The initial slope of the  $M_v(H)$  curves is larger than the value  $-1$  expected for perfect diamagnetism, which indicates non-zero demagnetization effects. The shape of the  $M_v(H)$  curves in Fig. 9 for  $\text{OsB}_2$  are suggestive of Type-I superconductivity with demagnetization effects. The hysteretic  $M_v(H)$  loops, shown in Figs. 10(a) and (b), were measured at  $1.7$  K with the magnetic field applied parallel and perpendicular, respectively to the length of the sample as shown in the insets in Figs. 10(a) and (b). The sample is a parallelopiped with dimensions length =  $3.25$  mm, width =  $1.57$  mm and thickness =  $0.35$  mm. There is a large irreversibility due to strong pinning in both measurements. We obtain an estimate of the reversible part of the magnetization  $M_{\text{rev}}$  by taking an average of the magnetization measured upon increasing and decreasing  $H$  between  $-100$  Oe and  $100$  Oe. The normalized  $M_{\text{rev}}$  obtained from the data in Fig. 10(a) is shown in 10(c) and  $M_{\text{rev}}$  obtained from the data in Fig. 10(b) is shown in 10(d). The data in Fig. 10(c) look like reversible magnetization curves for a Type-I superconductor with demagnetization effects, similar to the data in Fig. 9 above. The data in Fig. 10(d) are too noisy to draw conclusions. However, additional measurements and analysis suggest instead that  $\text{OsB}_2$  is a Type-II superconductor (see below), with a Ginzburg-Landau parameter  $\kappa$  on the Type-II side of the borderline between Type-I and Type-II superconductivity. The  $M_v(H)$  in Fig. 9 and Fig. 10, are however quite different from those expected for a Type-II superconductor,<sup>25</sup> an issue that needs to be addressed in future work.

From the  $M_v(H)$  curves in Fig. 9 we have estimated the critical field  $H_{c2}(T)$  from the construction in Fig. 9, illustrated for  $T = 1.7$  K. The  $H_{c2}(T)$  has been determined

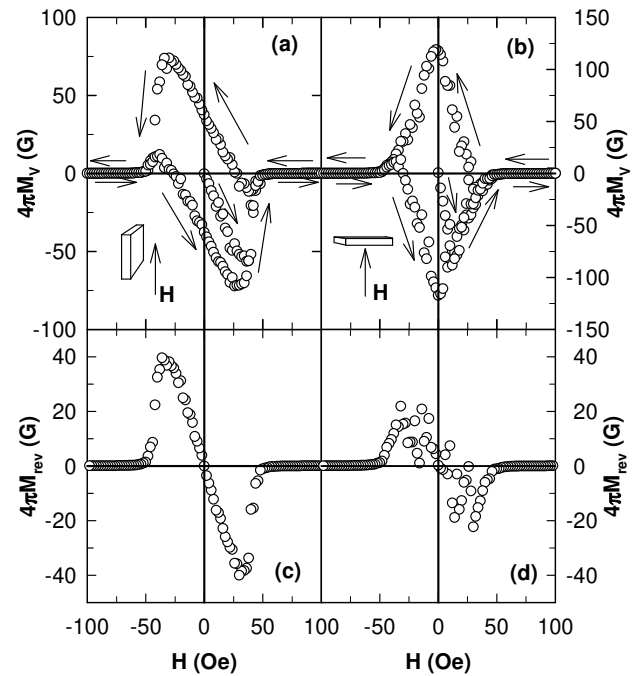


FIG. 10: (a) Hysteresis loop of the volume magnetization  $M_v(H)$  normalized by  $1/4\pi$ , versus applied magnetic field  $H$  at  $1.7$  K. The magnetic field is applied parallel to the length of the sample as shown in the inset. The arrows next to the data indicate the direction of field ramping during the measurement. (b) Hysteresis loop of the volume magnetization  $M_v(H)$  normalized by  $1/4\pi$ , versus applied magnetic field  $H$  at  $1.7$  K. The magnetic field is applied perpendicular to the length of the sample as shown in the inset. (c) The normalized reversible magnetization  $M_{\text{rev}}$  for the data shown in (a). (d) The normalized reversible magnetization  $M_{\text{rev}}$  for the data shown in (b).

by fitting a straight line to the data for a given temperature in the superconducting state and to the data in the normal state and taking the field  $H$  at which these lines intersect as the critical field at that temperature  $H_{c2}(T)$ .

The dynamic ac susceptibility  $\chi(T)$  data measured between  $0.5$  K and  $2.2$  K at a frequency of  $10$  MHz in various applied magnetic fields is shown in Fig. 11. To determine  $H_{c2}(T)$  from the data in Fig. 11 we have fitted a straight line to the data in the normal state and to the data below  $T_c$  for a given applied magnetic field and taken the value of the  $T$  at which these lines intersect as the  $T_c(H)$ . This is shown in Fig. 11 for the data at  $H = 0$ . By inverting  $T_c(H)$  we obtain  $H_{c2}(T)$ . The  $H_{c2}$  has also been obtained in a similar way from the  $\chi(T) \equiv M(T)/H$  SQUID magnetometer data (not shown here) between  $1.7$  K and  $2.4$  K in various applied magnetic fields. From the  $\rho(T)$  measurements [see Fig. 7(b)] the applied magnetic field has been taken to be the  $H_{c2}$  for the temperature at which the resistance drops to zero.

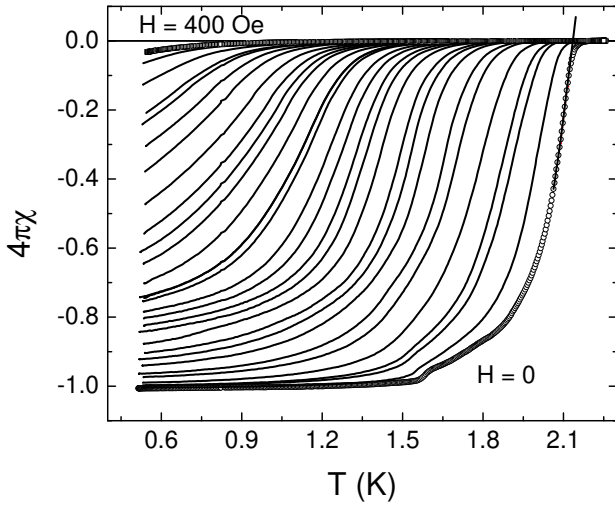


FIG. 11: Dynamic susceptibility  $\chi$  normalized to  $1/4\pi$ , versus temperature  $T$  at a frequency of 10 MHz with various applied magnetic fields  $H$ . The data have been normalized to a minimum value of -1 at the lowest  $T$ .

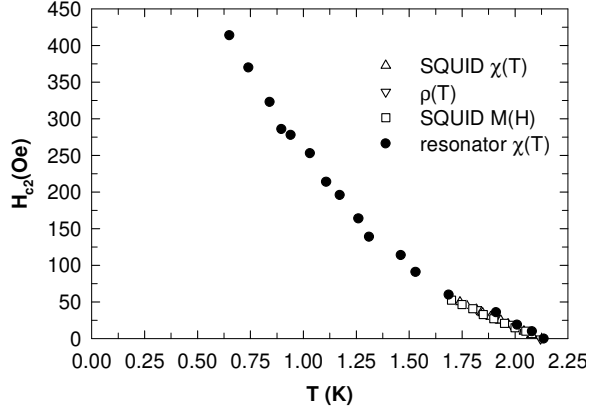


FIG. 12: Upper critical magnetic field  $H_{c2}$  versus temperature  $T$  extracted from four different types of measurements.

### 3. Analysis and Discussion of $H_{c2}(T)$ and Superfluid Density

The data for  $H_{c2}(T)$  obtained from all the measurements are plotted in Fig. 12. In the temperature range of the SQUID magnetometer measurements (1.7 K to 2.4 K) all the data match well and the temperature dependence of  $H_{c2}$  is linear. However, there is an upward curvature in  $H_{c2}(T)$  at lower temperatures as seen in the  $H_{c2}(T)$  data extracted from the ac  $\chi(T)$  measurements. This upward curvature is not unusual and is sometimes seen in unconventional superconductors<sup>26,27</sup> and also in the multi-band superconductor MgB<sub>2</sub>.<sup>28</sup> The reason for the positive curvature in  $H_{c2}(T)$  for OsB<sub>2</sub> needs to be investigated.

The temperature dependence of the change in London penetration depth,  $\Delta\lambda(T) = \lambda(T) - \lambda(T_{\min}) = \lambda(T) - \lambda(0.52 \text{ K})$ , is obtained from the  $\chi(T)$  data at  $H = 0$  in

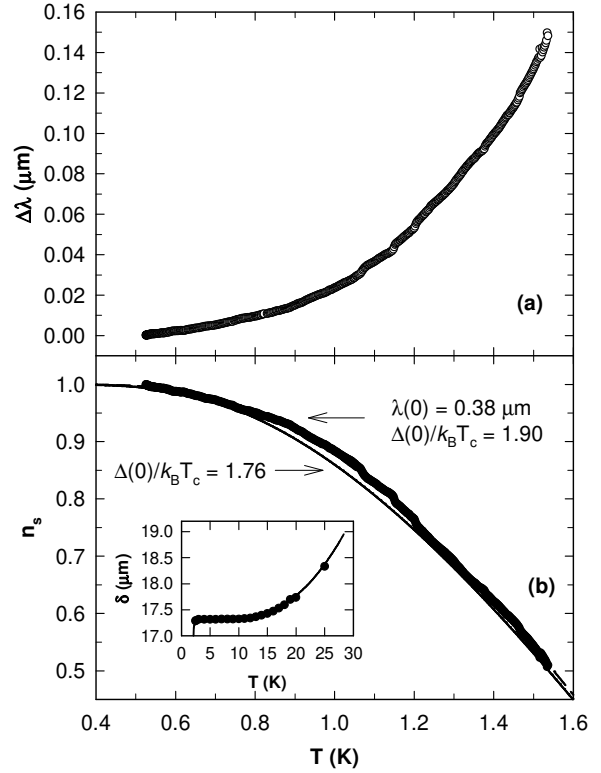


FIG. 13: (a) The temperature  $T$  dependence of the change  $\Delta\lambda$  in penetration depth in zero magnetic field  $\Delta\lambda(T) \equiv \lambda(T) - \lambda(0.52 \text{ K})$ . (b) The temperature dependence of the superfluid density  $n_s(T)$  of OsB<sub>2</sub>. The solid circles are the data, the dashed line is a fit by the standard  $s$ -wave BCS model where the superconducting gap  $\Delta(0)$  was allowed to vary and the solid line is a fit by the standard  $s$ -wave BCS model with the gap fixed to the weak-coupling BCS value  $\Delta(0) = 1.76 k_B T_c$ . The inset shows the calibrated normal-state skin-depth (solid curve) compared to the data from resistivity measurements (solid circles).

Fig. 11 using Eq. (1). The result is shown in Fig. 13(a). The temperature dependence of the superfluid density  $n_s(T)$  (the fraction of condensed electrons) can be obtained from the London penetration depth  $\lambda$  using the relation<sup>29</sup>

$$n_s = \left[ \frac{\lambda(0)}{\lambda(T)} \right]^2. \quad (14)$$

The  $n_s$  can be written in terms of the measured change in London penetration depth  $\Delta\lambda(T)$  as

$$\Delta\lambda(T) = \lambda(T) - \lambda(0.52 \text{ K}) = \lambda(0) \left( \frac{1}{\sqrt{n_s}} - C \right), \quad (15)$$

where  $C = \lambda(0.52 \text{ K})/\lambda(0)$ . The superfluid density depends on the shape of the Fermi surface and the superconducting gap symmetry. If we assume a spherical Fermi surface and  $s$ -wave superconductivity for OsB<sub>2</sub>,  $n_s$  is just a function of temperature and the magnitude of the zero temperature superconducting gap  $\Delta(0)$ .<sup>12</sup> We

fit the  $\Delta\lambda(T)$  data shown in Fig. 13(a) using Eq. (15) with  $\lambda(0)$ ,  $C$  and  $\Delta(0)$  the fitting parameters where we use  $T_c \equiv 2.15$  K and the BCS expression for  $n_s(T, \Delta(0))$  within a semi-classical approximation.<sup>30,31</sup> The fit gave the value  $\lambda(0) = 0.38(2)$   $\mu\text{m}$ ,  $C = 1.003(2)$ , and a slightly enhanced value for the superconducting gap  $\Delta(0) = 1.90(5)$   $k_B T_c$ . Allowing  $T_c$  to vary in the fit gave no significant change to the above initially assumed value of  $T_c$ . The  $n_s(T)$  data obtained from the estimated value of  $\lambda(0)$  and the measured  $\Delta\lambda(T)$  using Eq. (14) are shown in Fig. 13(b). Figure 13(b) also shows the results of the full-temperature BCS calculations for a weak-coupling  $s$ -wave BCS model with a fixed gap  $\Delta(0) = 1.76$   $k_B T_c$  (solid curve) and the result for an  $s$ -wave BCS model with the above gap  $\Delta(0) = 1.90(5)$   $k_B T_c$  (dashed curve). The observed behaviors of  $\lambda(T)$  and  $n_s(T)$  are consistent with  $s$ -wave superconductivity.

We now give a thermodynamic argument in favor of Type-II superconductivity in OsB<sub>2</sub>. The zero temperature thermodynamic critical field  $H_c(0)$  of a superconductor is related to the zero temperature superconducting gap  $\Delta(0)$  by the expression<sup>32</sup>

$$\frac{H_c(0)^2}{8\pi} = \frac{N(\epsilon_F)\Delta(0)}{4}, \quad (16)$$

where  $N(\epsilon_F)$  is the density of states at the Fermi energy for both spin directions. For OsB<sub>2</sub>, from our heat capacity results one has  $N(\epsilon_F) = 1.1$  states/eV f.u. =  $6.4 \times 10^{33}$  states/erg cm<sup>3</sup>. Also, our penetration depth data gave  $\Delta(0)/k_B T_c = 1.90$  which gives  $\Delta(0) = 5.6 \times 10^{-16}$  erg. Therefore, Eq. (16) gives  $H_c(0) = 158$  G. However, from Fig. 12 the critical field is  $\geq 420$  Oe. Therefore the critical field shown in Fig. 12 cannot be  $H_c$ , it must be  $H_{c2}$ , and therefore OsB<sub>2</sub> is a Type-II superconductor.

One can estimate the Ginzburg-Landau parameter  $\kappa$  using the relation<sup>32</sup>

$$H_{c2} = \sqrt{2}\kappa H_c. \quad (17)$$

With the value  $H_c(0) = 158$  G obtained above and the value  $H_{c2}(0) \geq H_{c2}(0.52$  K) = 420 G, we get  $\kappa \geq 1.9$ . This value of  $\kappa$  supports our above thermodynamic argument and puts OsB<sub>2</sub> on the Type-II side of the borderline ( $\kappa = \frac{1}{\sqrt{2}}$ ) between Type-I and Type-II superconductivity.

The  $\kappa$  can also be estimated from the relation<sup>32</sup>

$$\kappa = \frac{\lambda}{\xi}. \quad (18)$$

For a Type-II superconductor, the coherence length  $\xi$  can be estimated from the measured  $H_{c2}$  using the Ginzburg-Landau relation<sup>32</sup>

$$H_{c2} = \phi_0/2\pi\xi^2 \quad (19)$$

where  $\phi_0 = hc/2e = 2.068 \times 10^{-7}$  G cm<sup>2</sup> is the flux quantum. Since we have  $H_{c2}(T)$ , we can get  $\xi(T)$  using Eq. (19) and hence  $\kappa(T) = \frac{\lambda(T)}{\xi(T)}$  from the measured

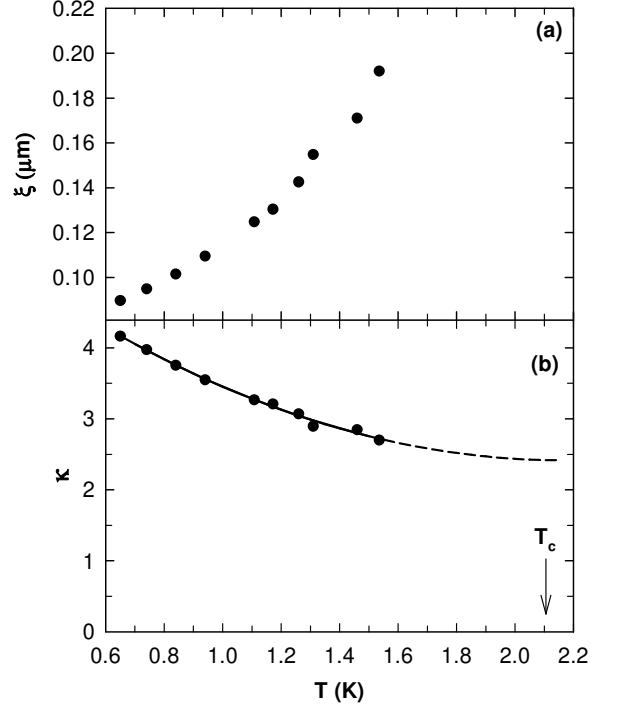


FIG. 14: (a) The temperature  $T$  dependence of the coherence length  $\xi$  and (b) of the Ginzburg-Landau parameter  $\kappa$ . The solid curve in (b) is a fit by a second order polynomial temperature dependence. The dashed line is an extrapolation up to  $T_c$  which is shown as the vertical arrow.

$\lambda(T)$ . The  $\xi(T)$  and  $\kappa(T)$  thus determined are shown in Fig. 14. Since the Ginzburg-Landau equations are written assuming a small order parameter, which means near  $T_c$ ,<sup>32</sup> the dividing line between Type-I and Type-II superconductivity being  $1/\sqrt{2}$  is defined near  $T_c$ . Therefore our  $\kappa(T)$  was fitted by a second order polynomial temperature dependence to get the extrapolated value  $\kappa(T_c = 2.14$  K) = 2.41(3). This value of  $\kappa$  is similar to the estimates made above. If the mean free path  $l$  could be made larger by improving the quality of the sample, OsB<sub>2</sub> has the potential to be a non-elemental Type-I superconductor.

#### IV. CONCLUSION

We have synthesized the compounds OsB<sub>2</sub> and RuB<sub>2</sub> and measured their magnetic, transport and thermal properties. Our measurements confirm that OsB<sub>2</sub> undergoes a bulk transition into the superconducting state below 2.1 K. Analysis of our data suggests that OsB<sub>2</sub> is a moderate-coupling ( $\lambda_{ep} = 0.4$  to 0.5) Type-II superconductor with a small Ginzburg-Landau parameter  $\kappa \sim 2$  and an upper critical field  $H_{c2}(0.5$  K)  $\sim 420$  Oe. The reduced specific heat anomaly at  $T_c$  and the positive curvature in  $H_{c2}(T)$  are similar to effects observed in MgB<sub>2</sub>. The temperature dependence of the superfluid density  $n_s(T)$  is consistent with an  $s$ -wave

superconductor with a slightly enhanced gap  $\Delta(0) = 1.90(5) k_B T_c$  and a zero temperature London penetration depth  $\lambda(0) = 0.38(2) \mu\text{m}$ . In the normal state OsB<sub>2</sub> and RuB<sub>2</sub> are Pauli paramagnetic metals with very similar properties: residual resistivity  $\rho_0 = 1.7(2)$  and  $1.1(1) \mu\Omega \text{ cm}$ ; Pauli susceptibility  $\chi_P = 3.4(5) \times 10^{-5}$  and  $5.22(7) \times 10^{-5} \text{ cm}^3/\text{mol}$ ; electronic specific heat coefficient  $\gamma = 1.90(1)$  and  $1.72(3) \text{ mJ/mol K}^2$ ; and low temperature  $T^3$  lattice specific heat coefficient  $\beta = 0.031(2)$  and  $0.015(1) \text{ mJ/mol K}^4$  for OsB<sub>2</sub> and RuB<sub>2</sub>, respectively. From our specific heat data, the density of states at the Fermi energy is  $N(\epsilon_F) = 1.1 \text{ states/(eV f.u.)}$  for OsB<sub>2</sub>. To investigate the effect of boron off-stoichiometry on the superconducting properties of OsB<sub>2</sub> we also investigated samples with starting compositions OsB<sub>1.9</sub> and OsB<sub>2.1</sub>. Both samples had a transition temperature  $T_c = 2.1 \text{ K}$  indicating no significant dependence of

$T_c$  on the boron stoichiometry. The diminished specific heat jump at  $T_c$  in Fig. 7(b), the non-Type-II shape of the superconducting  $M(H)$  in Fig. 9, and the positive curvature in  $H_{c2}(T)$  in Fig. 12, are all issues that require further investigation.

## Acknowledgments

We thank V. G. Kogan and P. C. Canfield for useful discussions. Ames Laboratory is operated for the U.S. Department of Energy by Iowa State University under Contract No. DE-AC02-07CH11358. This work was supported by the Director for Energy Research, Office of Basic Energy Sciences. R.P. also acknowledges support from NSF Grant number DMR-05-53285 and from the Alfred P. Sloan Foundation.

---

<sup>1</sup> J. Nagamastu, N. Nakagawa, T. Muranaka, Y. Zenitani, and J. Akimitsu, *Nature* **410**, 63 (2001).

<sup>2</sup> D. Kaczorowski, A. J. Zaleski, O. J. Zogal, and J. Klamut, *cond-mat/0103571*.

<sup>3</sup> V. A. Gasparov, N. S. Sidorov, I. I. Zverkova, and M. P. Kulakov, *JETP Lett.* **73**, 532 (2001).

<sup>4</sup> H. Rosner, W. E. Pickett, S.-L. Drechsler, A. Handstein, G. Behr, G. Fuchs, K. Nenkov, K.-H. Muller, and H. Eschrig, *Phys. Rev. B* **64**, 144516 (2001).

<sup>5</sup> A. S. Cooper, E. Corenzwit, L. D. Longinotti, B. T. Matthias, and W. H. Zachariasen, *Proc. Nat. Acad. Sci. USA* **67**, 313 (1970).

<sup>6</sup> N. I. Medvedeva, A. L. Ivanovskii, J. E. Medvedeva, and A. J. Freeman, *Phys. Rev. B* **64**, 020502(R) (2001).

<sup>7</sup> J. M. Vandenberg, B. T. Matthias, E. Corenzwit, and H. Barz, *Mater. Res. Bull.* **10**, 889 (1975).

<sup>8</sup> R. W. Cumberland, M. B. Weinberger, J. J. Gilman, S. M. Clark, S. H. Tolbert, and R. B. Kaner, *J. Am. Chem. Soc.*, **127**, 7264 (2005).

<sup>9</sup> M. Hebbachea, L. Stuparevi, and D. Zivkovi, *Solid State Commun.* **139**, 227 (2006).

<sup>10</sup> Z. Y. Chen, H. J. Xiang, J. Yang, J. G. Hou, and Q. Zhu, *Phys. Rev. B* **74**, 12102 (2006).

<sup>11</sup> L. Stuparevic and D. Zivkovic, *J. Therm. Anal. and Calor.* **76**, 975 (2004).

<sup>12</sup> For a topical review see R. Prozorov and R. W. Giannetta, *Supercond. Sci. Technol.* **19**, R41 (2006).

<sup>13</sup> R. Prozorov, R. W. Giannetta, A. Carrington, P. Fournier, R. L. Greene, P. Guptasarma, D. G. Hinks, and A. R. Banks, *Appl. Phys. Lett.* **77**, 4202 (2000).

<sup>14</sup> R. Prozorov, R. W. Giannetta, A. Carrington, and F. M. Araujo-Moreira, *Phys. Rev. B* **62**, 115 (2000).

<sup>15</sup> Rietveld analysis program DBWS-9807a release 27.02.99, ©1998 by R. A. Young, an upgrade of "DBWS-9411 - an upgrade of the DBWS programs for Rietveld Refinement with PC and mainframe computers, R.A. Young, *J. Appl. Cryst.* **28**, 366 (1995)".

<sup>16</sup> R. B. Roof Jr. and C. P. Kemper, *J. Chem. Phys.* **37**, 1473 (1962).

<sup>17</sup> R. E. Peierls, *Quantum Theory of Solids* (Clarendon Press, Oxford, 1955).

<sup>18</sup> R. D. Shannon, *Acta. Cryst.* **A32**, 751 (1976).

<sup>19</sup> S. Chiodo, H. J. Gotsis, N. Russo, and E. Sicilia, *Chem. Phys. Lett.* **425**, 311 (2006).

<sup>20</sup> L. B. Mendelsohn and F. Biggs, *Phys. Rev. A* **2**, 1130 (1970).

<sup>21</sup> C. Kittel, *Solid State Physics* (John Wiley and Sons, Inc., New York, 1966).

<sup>22</sup> S. L. Budko, G. Lapertot, C. Petrovic, C. E. Cunningham, N. Anderson, and P. C. Canfield, *Phys. Rev. Lett.* **86**, 1877 (2001).

<sup>23</sup> W. L. McMillan, *Phys. Rev.* **167**, 331 (1967).

<sup>24</sup> W. E. Pickett, *Braz. J. Phys.* **33**, 695 (2003).

<sup>25</sup> E. H. Brandt, *Phys. Rev. B* **68**, 054506 (2003).

<sup>26</sup> V. N. Zavaritsky, V. V. Kabanov, and A. S. Alexandrov, *Europhys. Lett.* **60**, 127 (2002).

<sup>27</sup> M. B. Maple, M. C. de Andrade, J. Herrmann, R. P. Dickey, N. R. Dilley, and S. Han, *J. Alloys and Comp.* **250**, 585 (1997).

<sup>28</sup> Z. X. Shi, M. Tokunaga, T. Tamegai, Y. Takano, K. Togano, H. Kito, and H. Ihara, *Phys. Rev. B* **68**, 104513 (2003).

<sup>29</sup> C. J. Gorter and H. Casimir, *Physica* **1**, 306 (1934).

<sup>30</sup> B. S. Chandrasekhar and D. Einzel, *Ann. Phys.* **2**, 535 (1993).

<sup>31</sup> R. Prozorov, T. A. Olheiser, R. W. Giannetta, K. Uozato, and T. Tamegai, *Phys. Rev. B* **73**, 184523 (2006).

<sup>32</sup> M. Tinkham, *Introduction to Superconductivity* (McGraw-Hill Inc., New York, 1975).